JACS
JOURNAL OF THE AMERICAN CHEMICAL SOCIETY
Article
pubs.acs.org/JACS

Simultaneous Discrimination of Diameter, Handedness, and Metallicity of Single-Walled Carbon Nanotubes with Chiral Diporphyrin Nanocalipers

Gang Liu,[†] Feng Wang,[†,⊥] Songpol Chaunchaiyakul,[§] Yukie Saito,[‡] Ajoy K. Bauri,[∥] Takahide Kimura,[†] Yuji Kuwahara,[§] and Naoki Komatsu*[,†]

[†]Department of Chemistry, Shiga University of Medical Science, Seta, Otsu 520-2192, Japan
[§]Department of Precision Science and Technology, Graduate School of Engineering, Osaka University, 2-1 Yamada-oka, Suita, Osaka 565-0871, Japan
[‡]Graduate School of Agricultural and Life Sciences, The University of Tokyo, 1-1-1 Yayoi, Bunkyo-ku, Tokyo 113-8657, Japan
[∥]Bio-Organic Division, Bhabha Atomic Research Center, Trombay, Mumbai 400085, India

Supporting Information

ABSTRACT: We have been developing the methodology to discriminate the handedness and diameter of single-walled carbon nanotubes (SWNTs) through molecular recognition using chiral diporphyrin nanotweezers. Although relatively small diameters of SWNTs (<1.0 nm) were recognized well, nanotweezers were not able to form stable complexes with the SWNTs having the diameters >1.0 nm. In this context, we designed chiral diporphyrin with a much larger cavity, namely, "nanocalipers". The feature of the newly designed host molecule is: (1) long spacer with more than 1.4 nm consisting of three aromatic moieties; (2) nearly parallel orientation of the two porphyrins; (3) restricted conformation by biaryl linkages of the porphyrin−carbazole and carbazole−anthracene; (4) strong interaction of two porphyrins and anthracene with the surface of a SWNT through $\pi-\pi$ stacking; and (5) stereogenic centers at the periphery of porphyrins discriminating helicity of SWNTs. As expected, we obtained optically active SWNTs with >1.0 nm in diameter and, unexpectedly, enriched metallic SWNTs over semiconducting ones. The optically active metallic SWNTs are identified for the first time, in addition to the optically active semiconducting SWNTs with such large diameters. The nanocalipers are found to recognize the diameter, handedness, and metallicity of SWNTs simultaneously.

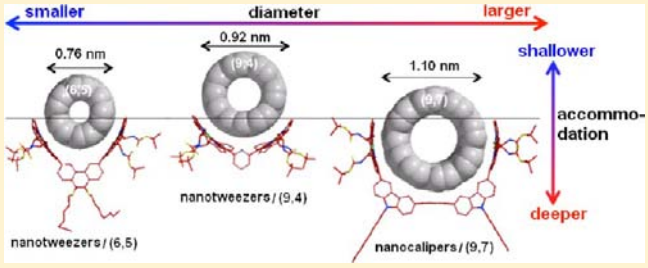

INTRODUCTION

Single-walled carbon nanotubes (SWNTs) have been attracting extensive interest due to their unique physical and chemical properties. However, the properties of SWNTs are known to strictly correlate with their structures,[1,2] encouraging separation of SWNTs according to their structures, such as diameter, length, roll-up index or (n,m), and handedness, and physical properties, such as metallicity.[3,4] Accordingly, several kinds of separation methods have been developed so far, such as electrophoresis, chromatography, density gradient ultracentrifugation (DGU), selective solubilization, and selective reaction.[3,4] As for optical resolution or handedness-based separation, preferential disperse[5] of either left- or right-handed SWNTs was achieved by use of "chiral diporphyrin nanotweezers" to give optically active SWNTs in 2007.[6] DGU using sodium cholate as chiral surfactant was also applied successfully to sort (n,m)-enantiomers, uncovering several kinds of optically active (n,m)-SWNTs.[7−9] Quite recently, chiral supramolecule and copolymers based on flavin mononucleotide and fluorene−binaphthol, respectively, were found to extract either left- or right-handed SWNTs preferentially through molecular recognition.[10,11] In the latter case, chiral fluorene−binaphthol copolymers also discriminated metallicity of SWNTs,[12] resulting in enrichment of optically active semiconducting SWNTs.[11]

In our previous works following the first report of the optically active SWNTs,[6] it was found that the chiral nanotweezers discriminate diameter and/or (n,m), in addition to handedness, of SWNTs according to the size and shape of the cleft made by two porphyrins and a spacer in between (Figure 1a,b).[4,13−18] Therefore, we have rationally designed several chiral nanotweezers to improve the selectivity toward (n,m) and handedness and realized single species enrichment, namely, enantiomers of (6,5)-SWNTs through complexation with **1** (Figure 1a).[16] It was rationalized that the nanotweezers with smaller dihedral angle made by two porphyrin units accepted smaller diameter of SWNTs deeply in the cleft,

Received: December 21, 2012
Published: March 4, 2013

ACS Publications © 2013 American Chemical Society

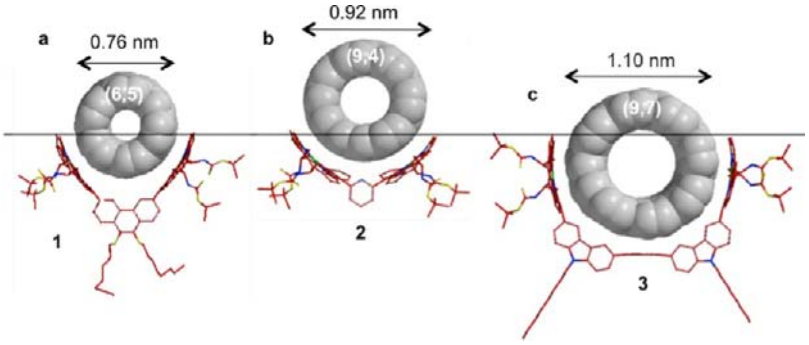

Figure 1. Computer-generated molecular modeling of the complex structures of (6,5)-, (9,4)-, and (9,7)-SWNTs with chiral diporphyrin nanotweezers **1** (a) and **2** (b) and nanocalipers **3** (c), respectively. The line is drawn to clarify the depth of SWNT accepted in the cleft of the host molecules. The two direction arrows and the values above the SWNTs indicate the diameters of these SWNTs.

Scheme 1. Synthesis of Chiral Diporphyrin Nanocalipers (*R*)- and (*S*)-3

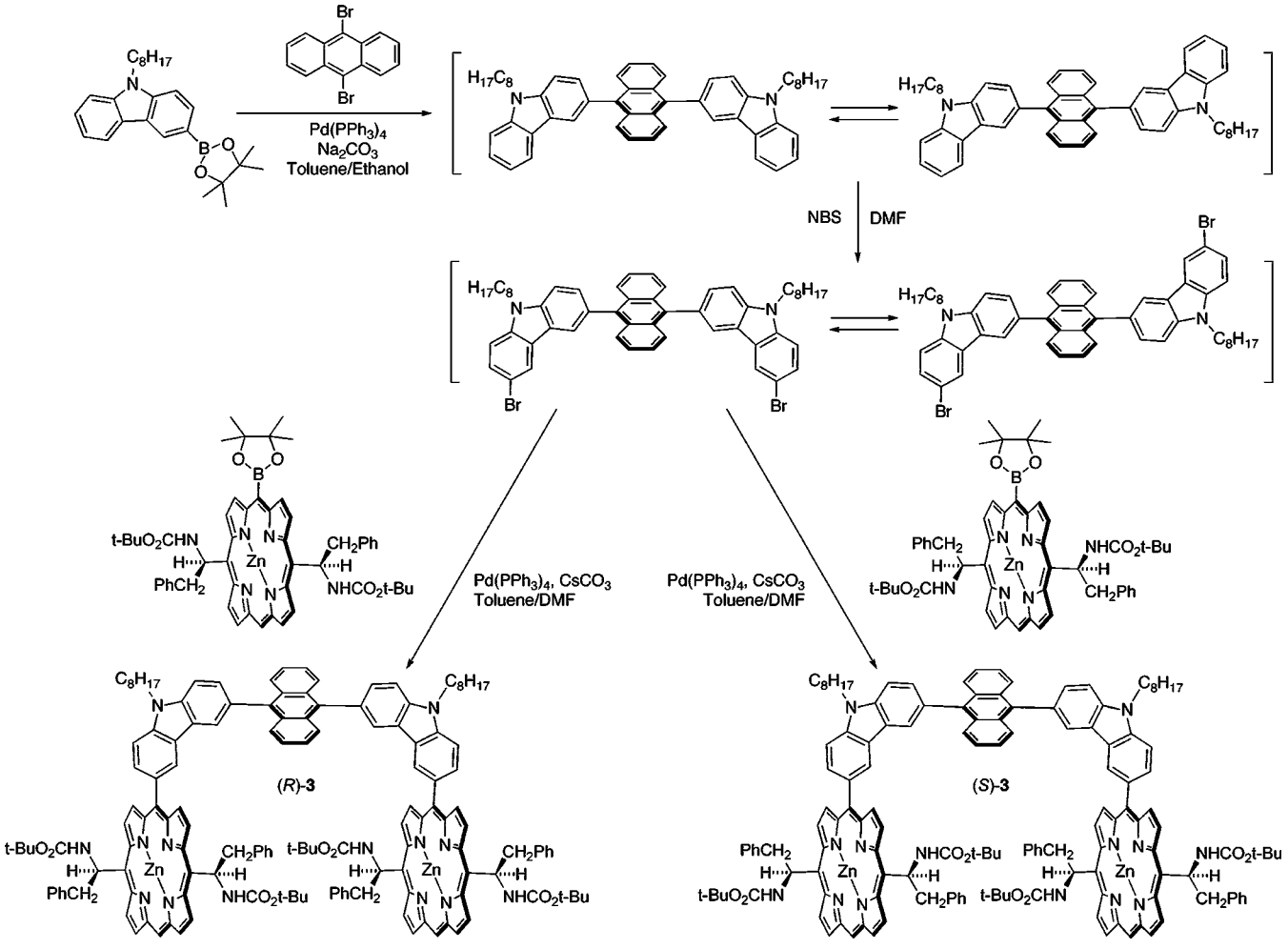

enabling precise differentiation of the diameter. In sorting of SWNTs with larger diameters, however, there has been limitation in selectivity by use of nanotweezers, because a larger dihedral angle, or shallow cavity, is needed to accept SWNTs with large diameters, decreasing the selectivity toward the diameter (Figure 1b).[15] It was concluded in our previous studies that the nanotweezers with the longer spacer and narrower angle exhibits better (*n*,*m*) selectivity than those with the shorter spacer and wider angle.[16] Based on this theory, "chiral diporphyrin nanocalipers" have been newly designed as shown in Figure 1c and Scheme 1. The points of this molecular design are: (1) much longer spacer (>1.4 nm) connecting three aromatic moieties directly; (2) nearly parallel orientation of the two porphyrins using two carbazoles at the edges of the spacer; (3) restricted conformation by biaryl linkages of the porphyrin−carbazole and carbazole−anthracene; (4) strong interaction of two porphyrins and anthracene with the surface of a SWNT through $\pi-\pi$ stacking; and (5) stereogenic centers at the periphery of porphyrins discriminating helicity of SWNTs. As we expected, optically active SWNTs with >1.0

dx.doi.org/10.1021/ja312519s | *J. Am. Chem. Soc.* 2013, 135, 4805−4814

nm in diameter were dominant after the extraction of SWNTs (HiPco) with the chiral nanocalipers **3**. Unexpectedly, we found that the nanocalipers recognize metallicity of SWNTs leading to enrichment of metallic SWNTs in the extract. The chiral nanocalipers are concluded to have multifunctions to recognize structural and physical properties of SWNTs, namely, helicity, diameter, and metallicity.

RESULTS AND DISCUSSION

Synthesis of Chiral Diporphyrin Nanocalipers. The chiral diporphyrin nanocalipers, (*R*)- and (*S*)-**3**, are synthesized as shown in Scheme 1. The long spacer consisting of three aromatics (carbazole−anthracene−carbazole) was prepared by Suzuki−Miyaura coupling of boronated carbazoles with dibromoanthracene. The two carbazoles bear long alkyl chains at the N-positions to increase solubility in organic solvents.[17] The three aromatic rings in the coupling product are conformationally restricted at the biaryl linkages, although they can rotate under ambient conditions.[19,20] Two carbazoles, perpendicular to anthracene, align almost in parallel in the most stable conformational isomers, enabling the parallel alignment of two porphyrins. The coupling product is considered to consist of the two conformational isomers in almost equal amounts, because the energy difference between the two conceivable isomers shown in Scheme 1 is calculated to be very small (<0.1 kJ mol^{-1} by molecular mechanics). After bromination of the spacer, two chiral porphyrins were coupled through the Suzuki−Miyaura coupling reaction. The product was identified as chiral diporphyrin nanocalipers by absorption, circular dichroism (CD), and ^{1}H and ^{13}C NMR spectroscopies (Figure 3a,b, and the Supporting Information). The nanocalipers should contain two conformational isomers, *syn* and *anti* forms. The *anti*-conformation is calculated to be more stable than the *syn*-one with a very small energy difference (0.16 kJ mol^{-1} by molecular mechanics). Since the aromatic rings can rotate as mentioned above, the *syn*-conformations of nanocalipers, (*R*)- and (*S*)-**3**, in Scheme 1 should be taken upon complexation with the SWNTs shown in Figure 1c.

Extraction of SWNTs with Chiral Diporphyrin Nanocalipers. First, 76-CoMoCAT (SWeNT SG-76 purchased from Sigma-Aldrich) was employed for the extraction; the SWNTs were bath sonicated in methanol in the presence of (*R*)-**3**, and the resulting black suspension was centrifuged. However, no SWNTs were extracted in the supernatant. The diameter of 76-CoMoCAT ranging from 0.7 to 1.1 nm was thought to be smaller than the size of the cavity in the nanocalipers, making the complex less stable. Second, we used SWNTs synthesized by arc discharge method (Honjo Chemical Co.), because the diameter (around 1.4 nm) is larger than that of 76-CoMoCAT. We failed to extract once again, probably because of too large diameters and/or tight bundling. Finally, HiPco (Carbon Nanotechnologies Inc.) was adopted due to larger diameter range, resulting in extraction of SWNTs with nanocalipers in methanol after high-speed centrifugation for two days (see the Experimental Section). The greenish extract was subjected to UV−vis−NIR, CD, and fluorescence spectroscopy measurements to confirm the existence of the complex between SWNTs and **3**, as depicted in Figure 1c.

In the fluorescence spectroscopy (Figure 2), the fluorescence intensity of the extract is much less than that of the nanocalipers at the excitation of 419 nm after normalization of the absorption at Soret band. Although SWNTs in the extract absorb and/or scatter the excitation (419 nm) and

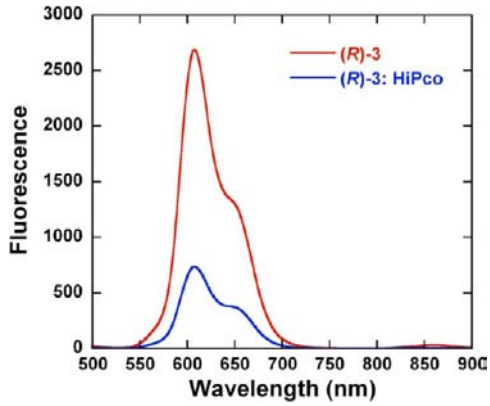

Figure 2. Fluorescence spectra of (*R*)-**3** in methanol and the extract. These solutions exhibited the same intensity (1.0 in Figure S6) of the absorption at 419 nm corresponding to the porphyrin Soret band.

emission (~600 nm) lights, this phenomenon can be interpreted by quenching of the excited porphyrins by SWNTs accommodated in the cavity of the nanocalipers (see the Supporting Information in detail), implying existence of the SWNT complex of **3**. After extraction of SWNTs, upward shift of the baseline and broad peak from 700 to 900 nm (E^{S}_{22} region shown in Figure 6) were observed in the absorption spectra shown in Figure 3a, supporting the above conclusion of existence of SWNTs in the extract. In addition, many strings, which seem to be individualized without bundling, are observed in the scanning transmission electron microscopy (STEM) and atomic force microscopy (AFM) of the extract as shown in Figures S1 and S2, respectively. It can be interpreted that each string of SWNT is individualized through complexation with nanocalipers not only in the solution phase (extract) but also in the solid phase after evaporating the solvent.

A broad peak appeared around 450 nm as a shoulder of the Soret band in the absorption spectra (Figure 3a), which may be caused by red shift of the Soret band through complexation. In that region, enhanced split CDs are observed in Figure 3b. Since fixation of the two porphyrin units in the diporphyrin complex is known to enhance the intensity of the split Cotton effects,[17,18,21] the split CDs are considered to be originated from the SWNT complexes of the nanocalipers, and hence the broad peak around 450 nm should correspond to the complex. Furthermore, the shoulder in the Soret band was deconvoluted into two peaks as shown in Figure 3c. These wavelengths are matched with those of the two deconvoluted peaks of the split CD in the extract (436 and 450 nm). The energy difference is known as Davydov splitting and is caused by exciton coupling.[22] The split Cotton effects were observed not only in the extract but also in the solutions of (*R*)- and (*S*)-**3**. The symmetrical positive and negative split CDs of (*R*)- and (*S*)-**3** and their SWNT complexes resulted from the exciton coupling of the two porphyrins located in the asymmetrical relationship.[21,23,24] In these exciton couplings, contribution from the SWNT excitons could be ignored, because the excitation at 450 nm generates a much lower number of excitons at SWNTs than that at porphyrins, because absorption due to SWNTs is much less than that of porphyrins at 450 nm as suggested by Figures 3a and 6. Since the positive and negative exciton-coupled CDs are reported to correspond to a clockwise and anticlockwise relationship between the two porphyrins,[22,23] (*R*)- and (*S*)-nanocalipers, exhibiting positive and negative split CDs, are suggested to adopt a clockwise and anticlockwise relationship,

dx.doi.org/10.1021/ja312519s | J. Am. Chem. Soc. 2013, 135, 4805−4814

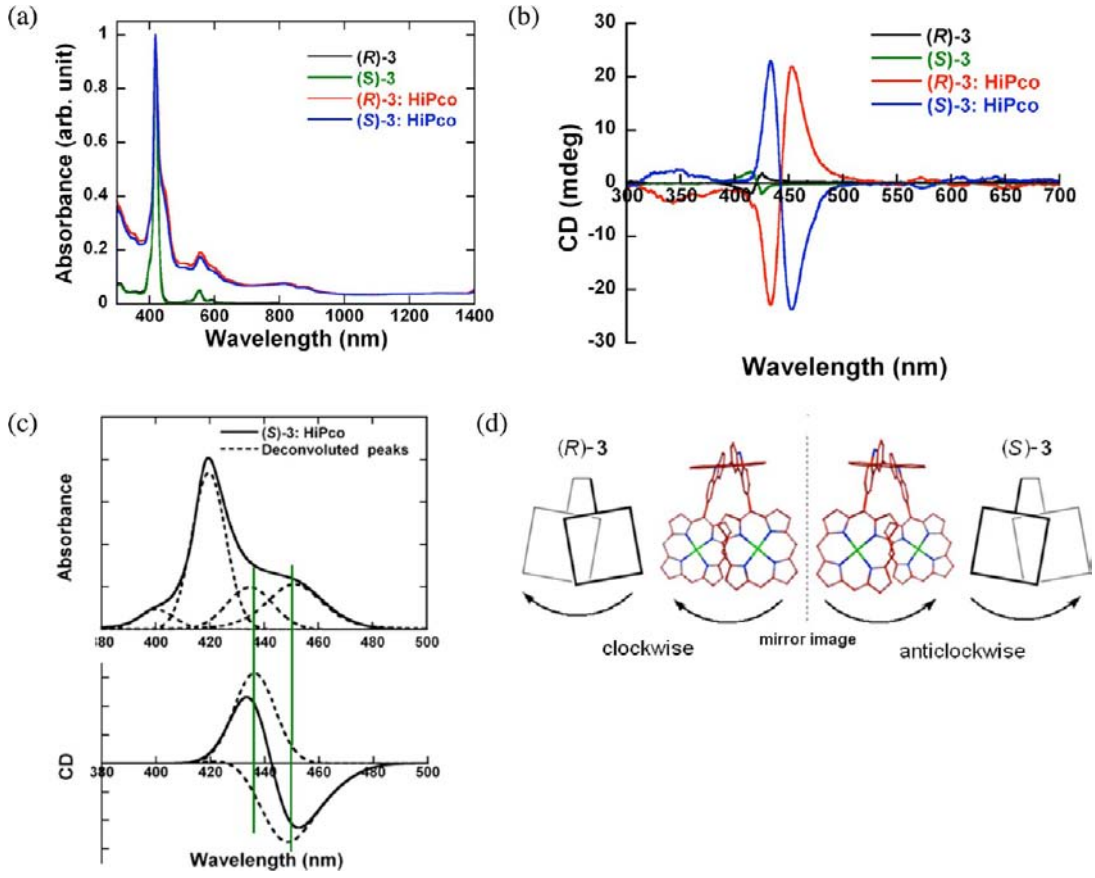

Figure 3. Absorption (a) and CD (b) spectra of (*R*)- and (*S*)-**3** before and after extraction. CD spectra of nanocalipers and nanocalipers−SWNT complexes were normalized at the absorbance of 419 and 450 nm (shoulder), respectively. (c) Deconvoluted (dotted lines) and experimentally obtained (solid lines) absortion and CD peaks of the extract from 380 to 500 nm after subtracting baseline. (d) Conformations of the nanocalipers before and after complexation suggested from the signs of the exciton couplings in the CD spectra. The substituents on the aromatic rings are omitted for clarity.

respectively, before and after complexation, as shown in Figure 3d. These asymmetric conformations are considered to be induced by the stereogenic centers at the periphery of the porphyrins. Based on these conformations of the nanocalipers, molecular modeling calculations (molecular mechanics) show that (*R*)- and (*S*)-**3** form more stable complexes with (*P*)- and (*M*)-(9,7)-SWNTs than (*M*)- and (*P*)-ones,[4,15] respectively, which will be mentioned below (Figure 8).

Complex Structure. Fluorescence quenching (Figure 2), red shift of the Soret band in the absorption spectrum (Figure 3a,c), and enhanced split Cotton effect in the CD spectra (Figure 3b,c) indicate the existence of the complex between SWNTs and the nanocalipers. In order to obtain direct evidence of the complex, we measured transmission electron microscopy (TEM, Figure 4a), AFM (Figure 4b), and scanning tunneling microscopy (STM, Figure 4c) of the SWNT extract with nanocalipers.

In the TEM image (Figure 4a), we could see something wrapping around the SWNTs. This is confirmed in the *z*-profile at AFM (Figure 4b). The height difference is observed even in the one string of SWNT. Relatively dark parts of the SWNT string (A−B and E−F in Figure 4b) exhibit 1.04−1.37 nm height (1.17 nm on average), which may correspond to the diameters of the bare SWNTs. On the other hand, the height of 1.90−2.34 nm (2.12 nm on average) is observed at the brighter part in the strings (C−D and G−H in Figure 4b). The average height difference between adjacent brighter and darker parts is calculated to be 0.97 nm. Since almost the same height difference was observed in the AFM of the SWNTs extracted with the nanotweezers,[17] we can conclude that the brighter and darker parts (2.12 and 1.17 nm in average height, respectively) in Figure 4b correspond to the individualized SWNTs coated and uncoated with nanocalipers, respectively. A closer view of the SWNT complex with nanocalipers was obtained by high resolution STM shown in Figure 4c. The 0.56 nm height difference between darker and brighter parts shown in the *z*-profile of I−J indicates the existence of the nanocalipers complexed with the SWNT. The two brightest parts, indicated in the red arrows in Figure 4c, and the less bright part in between may correspond to the two carbazoles and the anthracene, respectively, implying that the spacer of the nanocalipers is on the top of the SWNT. The discrepancy in the above height differences determined by AFM (0.97 nm) and STM (0.56 nm) might be attributed to the different orientation of the nanocalipers around the SWNT on the mica and HOPG substrates in the AFM and STM, respectively. The conceivable orientation of the complexes on the substrates is illustrated in Figure S3.

Selectivity toward Diameter and Metallicity of SWNTs. After concentration of the supernatants including the complex, the resulting solids were washed with THF and pyridine several times to thoroughly remove the nanocalipers from the complex. The washed samples were subjected to Raman spectroscopy (Figure 5) to determine the diameter

dx.doi.org/10.1021/ja312519s | *J. Am. Chem. Soc.* 2013, 135, 4805−4814

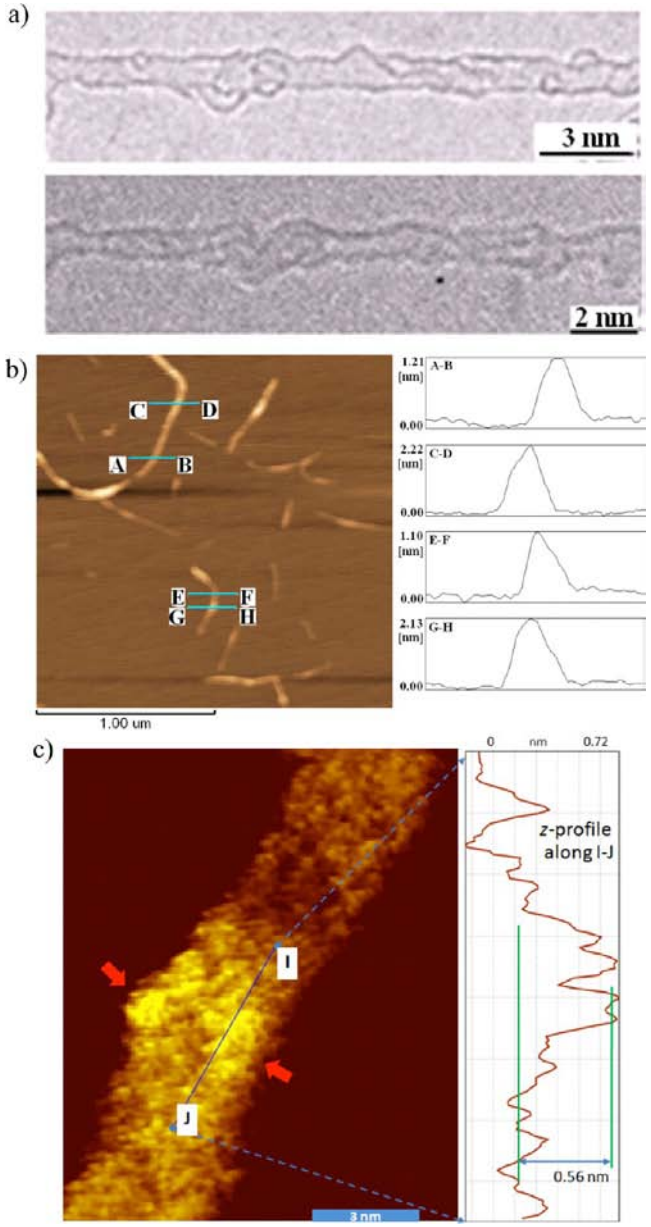

Figure 4. TEM (a), AFM (b), and STM (c) images of the SWNT complexes. *z*-Profiles along A–B, C–D, E–F, and G–H in the AFM image (b), and I–J in the STM image (c) are also added next to these images. Red arrows in (c) indicate the two brightest parts.

range enriched through the extraction with the nanocalipers. After the solid was dispersed in D_2O in the presence of achiral detergent, sodium dodecylbenzenesulfonate (SDBS), the resulting dispersions were analyzed with absorption and CD spectroscopies (Figures 6 and 7, respectively). It is worth noting that the intensity of the photoluminescence (PL) of the D_2O dispersion of the extracted SWNTs was too low to determine the abundance of the semiconducting SWNTs, although we tried several times.

Raman spectra of SWNTs (HiPco) before and after extraction were measured at the excitation of 785, 633, and 488 nm (Figure 5), and the intensity of the observed peaks is compared as shown in Table 1. Since almost the same spectra were obtained in the SWNTs extracted with (*R*)- and (*S*)-**3**, we used results of (*R*)-**3** in Figure 5 and Table 1.

Remarkable diameter shift through the extraction is suggested in the radial breathing mode (RBM) at the excitation of 785 nm (Figure 5a and Table 1). SWNTs with relatively small diameters, (9,4), (10,2), and (8,6) with 0.88–0.97 nm, are the major components in the HiPco (59% based on Raman intensity). After the extraction, the abundance of these SWNTs decreases significantly to 8%, and instead SWNTs with larger diameters ranging from 1.05 to 1.17 nm increase from 30% to 82%. The abundance of (11,3) with 1.01 nm in diameter is almost the same before and after the extraction. These results based on the Raman spectra (Figure 5a) suggest that the nanocalipers recognize the diameter of SWNTs and form more stable complexes with SWNTs with relatively larger diameters (1.05–1.17 nm) than those with diameters <1.0 nm.

Although only semiconducting SWNTs were detected at the excitation of 785 nm, metallic SWNTs were also found in the RBM at the excitation of 633 nm as shown in Figure 5b. Drastic change in the spectra has been also seen in this excitation wavelength through the extraction (Figure 5b,d). In terms of diameter selectivity, SWNTs with relatively larger diameters (1.07–1.22 nm) significantly increase from 49% to 93%, and accordingly the abundance of the smaller diameters decreases from 51% to 7% (Table 1). A similar range of diameters (1.07–1.22 nm) to that shown in Figure 5a (1.05–1.17 nm) is enriched in Figure 5b, suggesting the diameter selectivity toward the relatively larger diameters of SWNTs mentioned above. From the viewpoint of metallicity, metallic SWNTs, (13,4), (12,3), and (13,1), are enriched significantly, which is supported by the more pronounced Breit–Wigner–Fano (BWF) feature of the extracted SWNTs in the G-band region shown in Figure 5d.[25] Since all the SWNTs with larger diameters excited at 633 nm are metallic, the selectivity toward metallicity is ambiguous in Figure 5b.

At the excitation of 488 nm, metallic SWNTs with smaller diameters, (7,7) and (8,5), can be found in Figure 5c. In the semiconducting region <230 cm^{-1}, a larger diameter is preferred to a smaller one, as in the case of the excitation of 785 and 633 nm. While the peaks corresponding to (12,2)- and (13,0)-SWNTs with smaller diameters (1.03–1.04 nm) almost disappear after the extraction, the peak intensity of (13,3) increases from 62% to 90%. Although the metallic SWNTs detected at this excitation wavelength, (7,7) and (8,5), possess smaller diameters (0.90–0.96 nm), this intensity slightly increases from 7% to 9%, suggesting that the nanocalipers have preference toward metallic SWNTs in addition to larger diameters of 1.07–1.22 nm on the basis of the results in the Raman spectra (Figure 5).

The absorption spectra shown in Figure 6 support the above conclusion of the selectivity toward larger diameters and metallic SWNTs. Since almost the same spectra were obtained in the SWNTs extracted with (*R*)- and (*S*)-**3**, we used results of (*R*)-**3** in Figure 6. In both E^S_{11} and E^S_{22} regions, the major peaks with relatively large intensity shift from the shorter wavelength to the longer one, indicating that SWNTs with larger diameters are enriched through the extraction. The absorbance in the E^M_{11} region and the degree of the baseline upward shift of the extracted SWNTs increased as compared with those of the HiPco SWNTs, suggesting the enrichment of the metallic SWNTs.[26−28] The change in the relative abundance of (*n*,*m*)-SWNTs through the extraction is summarized in Table 2. Regardless of the metallicity, SWNTs with diameters of 1.05–1.22 nm, from (10,5) to (13,4) in Table 2, increase in relative abundance after the extraction,

dx.doi.org/10.1021/ja312519s | *J. Am. Chem. Soc.* 2013, 135, 4805–4814

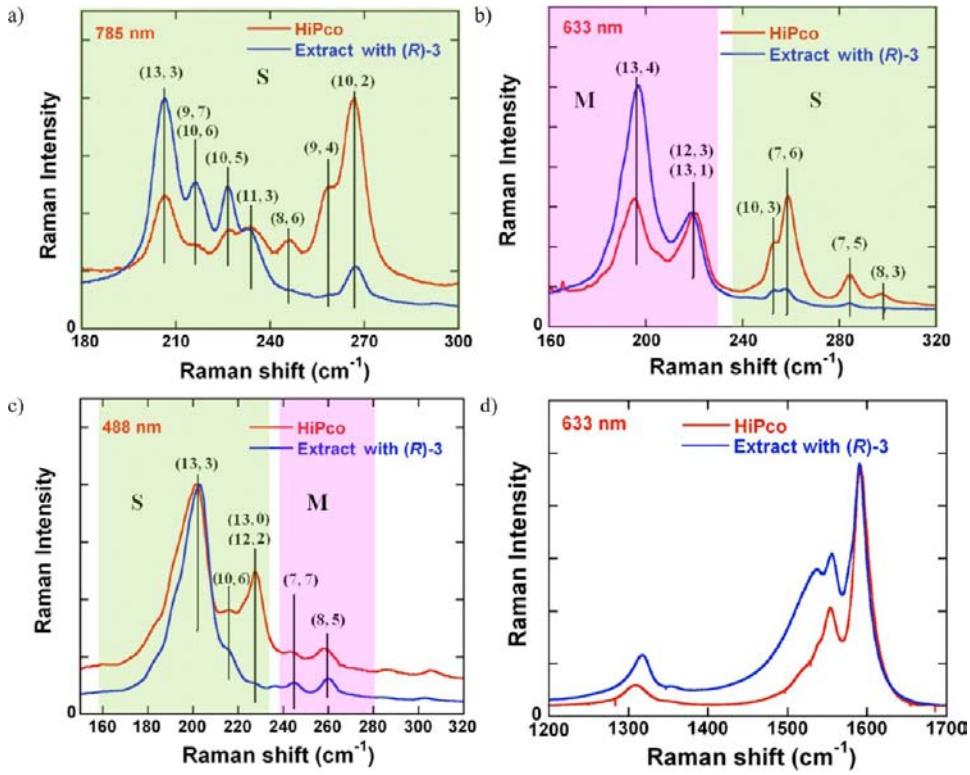

Figure 5. Raman spectra of SWNTs (HiPco) before and after the extraction with (*R*)-**3** in the region of RBM at the excitation of 785 (a), 633 (b), and 488 nm (c), and in the G band at the excitation of 633 nm (d). Green and pink regions indicate semiconducting (S) and metallic (M), respectively. The spectra were normalized at 233 (a), 220 (b), and 203 cm^{-1} (c), and the G band (d).

though that of (13,1) cannot be determined correctly because of the very steep absorption change in this region. On the contrary, the abundance of SWNTs with diameters smaller than 1.05 nm, from (12,2) to (8,3) in Table 2, relatively decrease except for metallic SWNTs, (9,6), (7,7), and (8,5). This shows that the nanocalipers recognize not only the diameters but also metallicity of SWNTs.

In order to make clear the preference for the metallic SWNTs, the baseline is subtracted in the E^{S}_{22} and E^{M}_{11} regions of the absorption spectra, and the abundance of the metallic and semiconducting SWNTs is compared, as shown in Figure S4a. It is found that the metallic SWNTs are significantly enriched through the extraction. In addition, the abundance of the metallic SWNTs in the supernatant was monitored at the duration of the centrifugation, 9, 25, and 45 h, as shown in Figure S4b. A significant increase in the abundance of the metallic SWNTs is confirmed at the 25 h centrifugation. Furthermore, the purple color of the D_2O dispersion of the extracted SWNTs shows the high concentration of the metallic SWNTs (Figure S5).[26,27] The enrichment of the metallic SWNTs may be a reason why no clear PL was observed in the PL spectra of the extracted SWNTs, as mentioned above. That is, the extracted SWNTs are considered to form small bundles after tip sonication followed by centrifugation, because of the tight bundling of the extracted SWNTs. Since the content of the metallic SWNTs is relatively large, most of the small bundles may contain metallic SWNTs to quench the PL from the semiconducting SWNTs included in the bundles. In addition, the metallic SWNTs exhibit no PL at the excitation of the wavelength of E^{S}_{22}.[1]

In our previous studies using the gable-type diporphyrins[18] and dipyrene[20] and monoporphyrin,[29] no significant enrichment of metallic or semiconducting SWNTs has been observed in the separation through molecular recognition. This indicates that these molecules did not recognize the metallicity of SWNTs. The nanocalipers are the first host molecule to recognize the metallicity of SWNTs in our studies. The parallel alignment of the two porphyrins in the nanocalipers and/or interaction of the anthracene with the SWNT surface (Figure 1c) might have a special effect to recognize the metallicity, which was not realized by the gable-type diporphyrins and monoporphyrin. A recognition of the metallicity of SWNTs with porphyrin was reported in 2004 by use of free-base tetraphenylporphyrin (TPP) derivative.[30] However, semiconducting SWNTs were preferentially extracted rather than metallic ones. Although we cannot interpret these opposite preference of nanocalipers and TPP derivative for metallic and semiconducting SWNTs, respectively, we would like to point out the structural difference between these porphyrins: TPP has four phenyl rings to prevent the porphyrin rings from sufficient direct interaction with the SWNT surface, while our porphyrin can face the SWNT surface, as shown in Figures 1 and 8, due to more flexible and less bulky substituents at the periphery of the porphyrins. In addition, the porphyrins in the nanocalipers include Zn as a central metal, while the TPP is a free base. Metallo- and free-base porphyrins have a difference in the structural rigidity and electrical property. These structural difference might cause the difference in the preference for the metallicity of SWNTs.

Optical Enrichment of SWNTs. The optical enrichment of the extracted SWNTs was confirmed by CD spectra, as shown in Figure 7. The SWNTs extracted with (*R*)- and (*S*)-**3** exhibit symmetrical CD peaks, indicating that the extracted SWNTs are optically active. Prominent peaks are indentified, as shown

dx.doi.org/10.1021/ja312519s | J. Am. Chem. Soc. 2013, 135, 4805−4814

Table 1. Comparison in Raman Intensity of (*n*,*m*)-SWNTs before and after the Extraction with Nanocalipers in the RBM

excitation wavelength (nm)	roll-up index[a]	diameter (nm)[b]	Raman shift (cm^{-1})[c]	Raman intensity before separation (%)[d]		Raman intensity after separation (%)[d]	
785	(13,3)	1.170	206 (204)	16	30	38	82
	(10,6), (9,7)	1.111, 1.103	216 (214, 216)	4		22	
	(10,5)	1.050	226–227 (226)	10		22	
	(11,3)	1.014	233–234 (233)	11	11	10	10
	(8,6)	0.966	246 (244)	6	59	1	8
	(9,4)	0.916	259 (256)	17		1	
	(10,2)	0.884	267 (264)	36		6	
633	(*13,4*)	1.222	197 (196)	26	49	64	93
	(*12,3*), (*13,1*)	1.091, 1.074	219–220 (218, 221)	23		29	
	(10,3)	0.936	253 (251)	15	51	3	7
	(7,6)	0.895	257–258 (261)	27		3	
	(7,5)	0.829	284 (281)	7		1	
	(8,3)	0.782	296–297 (297)	2		0	
488	(13,3)	1.170	203 (204)	62	62	90	90
	(10,6)	1.111	217 (214)	–		–	
	(12,2), (13,0)	1.041, 1.032	228 (227, 229)	31	31	1	1
	(7,7)	0.963	243–246 (244)	2	7	3	9
	(8,5)	0.902	258–261 (260)	5		6	

[a]Italic font (*n*,*m*) indicates metallic SWNTs, while regular font (n,m) is semiconducting SWNTs. [b]Refs 31 and 32. [c]Raman shifts in parentheses are the reported ones.[33] [d]Raman intensity was determined in the Raman spectra shown in Figure 5a–c. Value in the right column is the subtotal in each section.

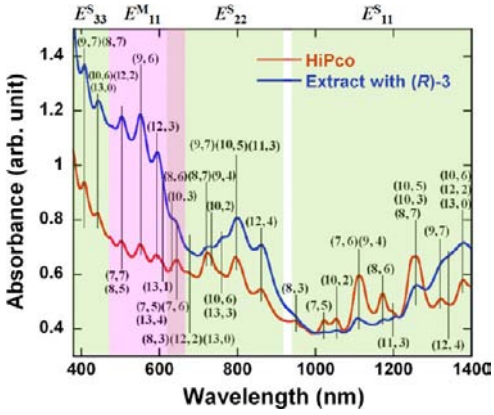

Figure 6. Absorption spectra of D_2O dispersions of SWNTs in the presence of SDBS before and after extraction with (*R*)-**3**. Green and pink regions indicate semiconducting (S) and metallic (M), respectively.

in Figure 7. Since no clear and symmetrical CD is observed in the wavelength of 300–400 nm and 900–1100 nm, the semiconducting SWNTs having absorption in these ranges (Table 2) are not considered for the assignment of the CDs (Figure 7). These assigned SWNTs exhibiting prominent CDs are the SWNTs enriched in their abundance through the extraction except for (8,7)-SWNTs (Table 2).

Although many optically active SWNTs have been identified so far by CD, all of them are semiconducting SWNTs with diameters <1.0 nm.[4,8,15] In contrast, all the (*n*,*m*)-SWNTs exhibiting prominent CDs in Figure 7 have diameters >1.0 nm, owing to the preference of the nanocalipers for SWNTs with relatively large diameters as described above. This indicates that all of them are newly identified optically active SWNTs. In addition, optically active metallic SWNTs are identified for the first time thanks to the significant enrichment of the matallic SWNTs through the extraction with the nanocalipers mentioned above.

In order to correlate the helicity of a SWNT (*M* or *P*) with the sign (positive or negative) in CD, we carried out molecular modeling calculations (molecular mechanics) for the 1:1 complexes of (*R*)- and (*S*)-**3** with (*P*)- and (*M*)-(9,7)-SWNTs. The energy-minimized structures are shown in Figure 8, where the conformations of (*R*)- and (*S*)-**3** are clockwise and anticlockwise, respectively, determined by the CDs of the complexes mentioned above (Figure 3b,d). Although the energy difference is not so large (0.72 kJ mol^{-1}), (*R*)-**3**/(*P*)-

dx.doi.org/10.1021/ja312519s | *J. Am. Chem. Soc.* 2013, 135, 4805–4814

Table 2. Comparison in Absorbance of (*n,m*)-SWNTs before and after the Extraction with Nanocalipers

roll-up index[a]	diameter (nm)[b]	E^S_{11} (nm)[c]	E^S_{22} (nm)[c]	E^S_{33} (nm)[d]	E^M_{11} (nm)[c]	relative abundance[e]
(*13,4*)	1.222				644 (640)	+
(13,3)	1.170	– (1497)	767 (764)			+
(12,4)	1.145	1345 (1342)	862 (867)			+
(10,6)	1.111	1379 (1380)	767 (758)	444 (439)		+
(9,7)	1.103	1322 (1323)	799 (799)	408 (406)		+
(*12,3*)	1.091				595 (598)	+
(*13,1*)	1.074				609 (600)	±
(10,5)	1.050	1260 (1250)	799 (795)	– (379)		+
(12,2)	1.041	1379 (1376)	673 (683)	444 (454)		–
(*9,6*)	1.038				551 (551)	+
(8,7)	1.032	1260 (1267)	723 (732)	408 (404)		–
(13,0)	1.032	1379 (1384)	673 (672)	444 (456)		–
(11,3)	1.014	1200 (1197)	799 (798)	– (384)		±
(8,6)	0.966	1172 (1172)	723 (722)	– (370)		–
(*7,7*)	0.963				504 (505)	+
(10,3)	0.936	1260 (1250)	632 (628)			–
(9,4)	0.916	1108 (1101)	723 (724)	– (362)		–
(*8,5*)	0.902				504 (506)	+
(7,6)	0.895	1108 (1122)	644 (650)	– (371)		–
(10,2)	0.884	1053 (1053)	727 (735)	– (372)		–
(7,5)	0.829	1023 (1023)	644 (647)	– (337)		–
(8,3)	0.782	949 (952)	673 (661)	– (351)		–

[a]Italic font (*n, m*) indicates metallic SWNTs, while regular font (n,m) is semiconducting SWNTs. [b]Refs 31 and 32. [c]Wavelengths are determined in the absorption spectra shown in Figure 6. Wavelengths in parentheses are the reported ones.[33] The peaks in the range of wavelength shorter than 400 nm were not seen behind high and/or steep background and are indicated as "–". [d]Ref 34. [e]Signs of "+", "–", and "±" indicate that the abundance of the given (*n,m*)-SWNTs relatively increase, decrease, and cannot be determined, respectively.

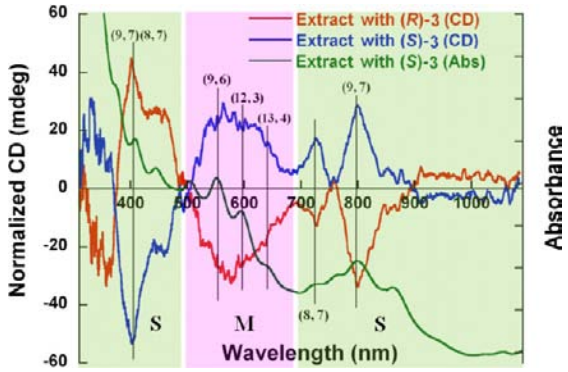

Figure 7. CD spectra of SWNTs extracted with (*R*)- and (*S*)-**3** and absorption spectra of SWNTs extracted with (*S*)-**3**. CD spectra are normalized at the absorption at 551 nm. The CD spectra at 300–500 and 500–1100 nm were taken using different spectrophotometers. Green and pink regions indicate semiconducting (S) and metallic (M), respectively.

(9,7) and (*S*)-**3**/(*M*)-(9,7) are more stable than (*R*)-**3**/(*M*)-(9,7) and (*S*)-**3**/(*P*)-(9,7), implying that (*P*)-(9,7)-SWNTs exhibit positive and negative CDs in the regions of E^S_{33} and E^S_{22}, respectively, and (*M*)-(9,7)-SWNTs do opposite signs, as shown in Figure 7.

CONCLUSION

Based on the previous research on the chiral nanotweezers, we rationally designed the chiral diporphyrin nanocalipers and employed them for the SWNT separation. In the molecular design, the two chiral porphyrin units align in parallel through the spacer consisting of three aromatic sequence, carbazole–anthracene–carbazole, with >1.4 nm in length. The much deeper and larger cavity of the nanocalipers than nanotweezers enabled to accommodate SWNTs with larger diameters (>1.0 nm) and to discriminate the handedness of SWNTs, as we intended in the molecular design. An additional property of nanocalipers, which has not been observed in the nanotweezers,

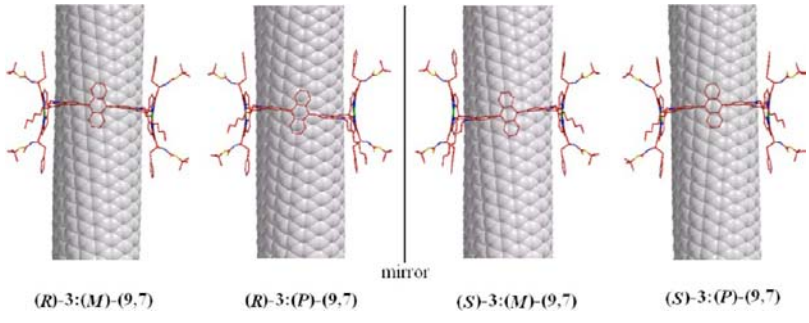

Figure 8. Computer-generated molecular modeling of the complex structures of 1:1 complexes of (*R*)- and (*S*)-**3** with (*P*)- and (*M*)-(9,7)-SWNTs. The clockwise and anticlockwise conformations shown in Figure 3d are adopted for (*R*)- and (*S*)-**3**, respectively.

dx.doi.org/10.1021/ja312519s | *J. Am. Chem. Soc.* 2013, 135, 4805–4814

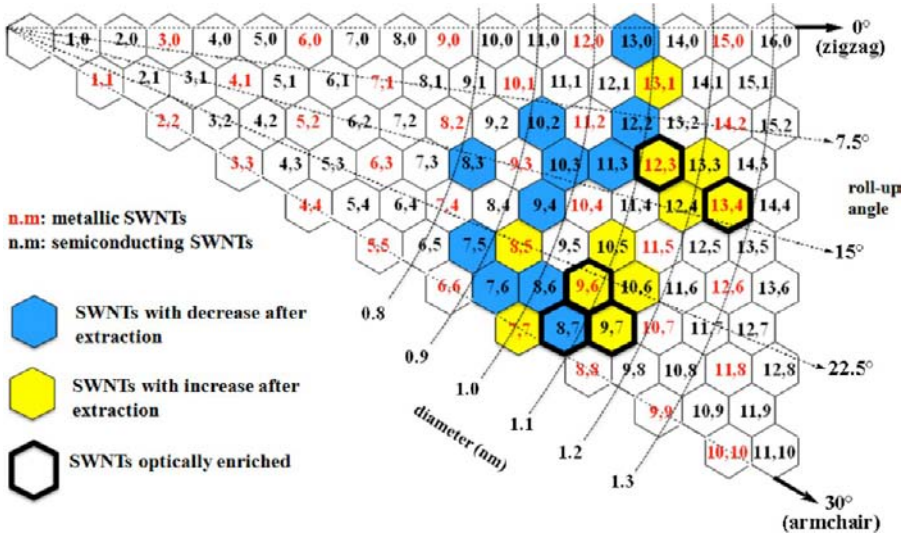

Figure 9. Summary in discrimination of diameter, handedness, and metallicity of SWNTs with chiral diporphyrin nanoclipers **3**.

is to discriminate the metallicity of SWNTs. These three functions to recognize diameter, handedness, and metallicity of SWNTs have been found in the nanocalipers, as summarized in Figure 9. The SWNTs with diameters >1.05 nm are enriched in their abundance regardless of the metallicity. Even if the diameters are <1.05 nm, metallic SWNTs are enriched slightly through the extraction with nanocalipers. As for the optical enrichment, the CDs of the semiconducting SWNTs with diameters >1.0 nm are identified for the first time, such as (9,7)- and (8,7)-SWNTs. In addition, optically active metallic SWNTs, such as (9,6)-, (12,3)-, and (13,4)-SWNTs, are also found for the first time.

EXPERIMENTAL SECTION

Extraction of HiPco-SWNTs with Nanocalipers. Chiral nanocalipers (*R*)- or (*S*)-**3** (10 mg) and HiPco-SWNTs (10 mg) in methanol (40 mL) were bath sonicated at 20 °C for 36 h. After centrifugation of the resulting suspension at 50 400*g* for 45 h, the supernatant was subjected to UV−vis−NIR, fluorescence, CD, TEM, AFM, STM, and STEM measurements. After concentration of the supernatant, the residual solid was washed with THF and pyridine several times until the porphyrin Soret band disappeared in the UV−vis spectra of the washings. The thoroughly washed SWNTs (0.65 mg) were analyzed with Raman spectroscopy at excitation of 488, 633, and 785 nm. The solid sample was dispersed in D_2O (16 mL) in the presence of SDBS (10 mg mL^{-1}) by bath sonication at 20 °C for 10 h and then tip sonication for 3 h at 0 °C. After centrifugation at 136 000*g* for 40 min, the upper layer (about 85%) of the supernatant was poured up and subjected to UV−vis−NIR and CD measurements. For the dispersion of the raw HiPco-SWNTs, tip sonication was carried out for 40 min under the same conditions followed by centrifugation at 543 000*g* for 60 min.

ASSOCIATED CONTENT

Supporting Information

Experimental details of the synthesis of the nanocalipers, interpretation for fluorescence quenching through complexation (Figures S6 and S7), STEM and AFM images (Figures S1 and S2), illustration of the complexes on the substrates (Figure S3), absorption spectra (Figure S4), photographs of the D_2O solutions of the SWNTs (Figure S5), and ^{13}C and ^{1}H NMR spectra (Figure S8). This material is available free of charge via the Internet at http://pubs.acs.org.

AUTHOR INFORMATION

Corresponding Author

nkomatsu@belle.shiga-med.ac.jp

Present Address

[⊥]Key Laboratory for Green Chemical Process of Ministry of Education, Wuhan Institute of Technology, Wuhan 430073, China.

Notes

The authors declare no competing financial interest.

ACKNOWLEDGMENTS

The authors thank Prof. Yasushi Kawai (Nagahama Institute of Bio-Science and Technology) and Prof. Hiroshi Imahori, Dr. Tomokazu Umeyama, and Dr. Tatsuya Murakami (Kyoto University) for allowing us to use CD spectropolarimeter and PL spectrophotometer, respectively. The authors are grateful to Prof. Kazunari Matsuda (Kyoto University) and Prof. Lorenzo Stella (Università di Roma Tor Vergata) for helpful suggestions about exciton coupling between SWNTs and porphyrin and fluorescence quenching of the complex, respectively. This work was financially supported by Grant-in-Aid for Scientific Research (S) (no. 24221009), Grant-in-Aid for Scientific Research on Priority Areas (no. 22016005), Grant-in-Aid for Scientific Research (B) (no. 23350062), the Kurata Memorial Hitachi Science and Technology Foundation, Adaptable and Seamless Technology Transfer Program through Target-driven R (JST), and Industrial Technology Research Grant Program in 2005 from New Energy and Industrial Technology Development Organization (NEDO) of Japan.

REFERENCES

(1) Kataura, H.; Kumazawa, Y.; Maniwa, Y.; Umezu, I.; Suzuki, S.; Ohtsuka, Y.; Achiba, Y. *Synth. Met.* **1999**, *103*, 2555.

(2) Strano, M. S.; Doorn, S. K.; Haroz, E. H.; Kittrell, C.; Hauge, R. H.; Smalley, R. E. *Nano Lett.* **2003**, *3*, 1091.

(3) Komatsu, N.; Wang, F. *Materials* **2010**, *3*, 3818.

(4) Liu, G.; Wang, F.; Peng, X.; Rahman, A. F. M. M.; Bauri, A. K.; Komatsu, N. In *Handbook of carbon nano materials*; D'Souza, F., Kadish, K. M., Eds.; World Scientific: Singapore, 2012; Vol. 3, p 203.

(5) Premkumar, T.; Mezzenga, R.; Geckeler, K. E. *Small* **2012**, *8*, 1299.

(6) Peng, X.; Komatsu, N.; Bhattacharya, S.; Shimawaki, T.; Aonuma, S.; Kimura, T.; Osuka, A. *Nat. Nanotechnol.* **2007**, *2*, 361.
(7) Green, A. A.; Duch, M. C.; Hersam, M. C. *Nano Res.* **2009**, *2*, 69.
(8) Ghosh, S.; Bachilo, S. M.; Weisman, R. B. *Nat. Nanotechnol.* **2010**, *5*, 443.
(9) Green, A. A.; Hersam, M. C. *Adv. Mater.* **2011**, *23*, 2185.
(10) Ju, S.-Y.; Abanulo, D. C.; Badalucco, C. A.; Gascón, J. A.; Papadimitrakopoulos, F. *J. Am. Chem. Soc.* **2012**, *134*, 13196.
(11) Akazaki, K.; Toshimitsu, F.; Ozawa, H.; Fujigaya, T.; Nakashima, N. *J. Am. Chem. Soc.* **2012**, *134*, 12700.
(12) Nish, A.; Hwang, J.-Y.; Doig, J.; Nicholas, R. J. *Nat. Nanotechnol.* **2007**, *2*, 640.
(13) Peng, X.; Komatsu, N.; Kimura, T.; Osuka, A. *J. Am. Chem. Soc.* **2007**, *129*, 15947.
(14) Peng, X.; Komatsu, N.; Kimura, T.; Osuka, A. *ACS Nano* **2008**, *2*, 2045.
(15) Peng, X.; Wang, F.; Bauri, A. K.; Rahman, A. F. M. M.; Komatsu, N. *Chem. Lett.* **2010**, *39*, 1022.
(16) Wang, F.; Matsuda, K.; Rahman, A. F. M. M.; Peng, X.; Kimura, T.; Komatsu, N. *J. Am. Chem. Soc.* **2010**, *132*, 10876.
(17) Wang, F.; Matsuda, K.; Rahman, A. F. M. M.; Kimura, T.; Komatsu, N. *Nanoscale* **2011**, *3*, 4117.
(18) Liu, G.; Yasumitsu, T.; Zhao, L.; Peng, X.; Wang, F.; Bauri, A. K.; Aonuma, S.; Kimura, T.; Komatsu, N. *Org. Biomol. Chem.* **2012**, *10*, 5830.
(19) Meyers, A. I.; Himmelsbach, R. J. *J. Am. Chem. Soc.* **1985**, *107*, 682.
(20) Rahman, A. F. M. M.; Wang, F.; Matsuda, K.; Kimura, T.; Komatsu, N. *Chem. Sci.* **2011**, *2*, 862.
(21) Borovkov, V. V.; Hembury, G. A.; Inoue, Y. *Acc. Chem. Res.* **2004**, *37*, 449.
(22) Harada, N.; Nakanishi, K. *Circular dichroic spectroscopy-exciton coupling in organic stereochemistry*; University Science Books: Mill Valley, CA, 1983.
(23) Tsubaki, K.; Takaishi, K.; Tanaka, H.; Miura, M.; Kawabata, T. *Org. Lett.* **2006**, *8*, 2587.
(24) Matile, S.; Berova, N.; Nakanishi, K.; Fleischhauer, J.; Woody, R. W. *J. Am. Chem. Soc.* **1996**, *118*, 5198.
(25) Brown, S. D. M.; Jorio, A.; Corio, P.; Dresselhaus, M. S.; Dresselhaus, G.; Saito, R.; Kneipp, K. *Phys. Rev. B* **2001**, *63*, 155414.
(26) Tanaka, T.; Urabe, Y.; Nishide, D.; Kataura, H. *Appl. Phys. Express* **2009**, *2*, 125002.
(27) Maeda, Y.; Kimura, S.; Kanda, M.; Hirashima, Y.; Hasegawa, T.; Wakahara, T.; Lian, Y.; Nakahodo, T.; Tsuchiya, T.; Akasaka, T.; Lu, J.; Zhang, X.; Gao, Z.; Yu, Y.; Nagase, S.; Kazaoui, S.; Minami, N.; Shimizu, T.; Tokumoto, H.; Saito, R. *J. Am. Chem. Soc.* **2005**, *127*, 10287.
(28) Naumov, A. V.; Ghosh, S.; Tsyboulski, D. A.; Bachilo, S. M.; Weisman, R. B. *ACS Nano* **2011**, *5*, 1639.
(29) Peng, X.; Wang, F.; Komatsu, N.; Kimura, T.; Osuka, A. *J. Phys. Chem. C* **2009**, *113*, 9108.
(30) Li, H.; Zhou, B.; Lin, Y.; Gu, L.; Wang, W.; Fernando, K. A. S.; Kumar, S.; Allard, L. F.; Sun, Y.-P. *J. Am. Chem. Soc.* **2004**, *126*, 1014.
(31) Weisman, R. B.; Bachilo, S. M. *Nano Lett.* **2003**, *3*, 1235.
(32) Strano, M. S.; Doorn, S. K.; Haroz, E. H.; Kittrell, C.; Hauge, R. H.; Smalley, R. E. *Nano Lett.* **2003**, *3*, 1091.
(33) Nanot, S.; Hároz, E. H.; Kim, J.-H.; Hauge, R. H.; Kono, J. *Adv. Mater.* **2012**, *24*, 4977.
(34) Haroz, E. H.; Bachilo, S. M.; Weisman, R. B.; Doorn, S. K. *Phys. Rev. B* **2008**, *77*, 125405.